ISSN 2321-807X

The effect of pH and the process of direct or inverse synthesis of silicon-Substituted hydroxyapatite prepared by hydrolysis in aqueous medium

Bochra DHOUIB [a] , Noureddine Jouini [b], Farah Karmous [b], Ovidiu brinza [b],
Fréderic Schoenstein [b], Hafed El Feki [a*]

[a] Laboratoire des Sciences des Matériaux et d'Environnements, Faculté des Sciences de Sfax, B.P.n° 802-3000 Sfax, Tunisie.
E-mail : dhouibbochra86@yahoo.fr
[b] Laboratoire des Sciences des Procédés et des Matériaux, CNRS-UPR 9001, Université Paris 13, PRES Sorbonne Paris Cité, 93430 Villetaneuse, France.
E-mail : nourredine.jouini@lspm.cnrs.fr
E-mail : farah.karmous@lspm.cnrs.fr
E-mail : ovidiu.brinza@lspm.cnrs.fr
E-mail : frederic.schoenstein@lspm.cnrs.fr
E-mail : hafed.elfeki@yahoo.fr
*Corresponding author: E-mail address: hafed.elfeki@yahoo.fr

ABSTRACT

Nanosized hydroxyapatite with silicon substitution $Ca_{10}(PO_4)_{6-x}(SiO_4)_x(OH)_{2-x}\square_x$ ($0 \leq x \leq 2$) of same silicon concentrations, variation of pH and the method of inverse and direct synthesis were successfully prepared first time by the theoretical maximum of incorporation of Si into the hexagonal apatite structure by precipitation method aqueous. The effects of the Si substitution on crystallite size, particle size and morphology of the powders were investigated. The crystalline phase, microstructure, morphology and particle size of hydroxyapatite and silicon substituted hydroxyapatites were characterized by X-ray diffraction (XRD), Fourier transform infrared spectroscopy (FTIR), scanning electron microscopy (SEM), EDX coupled with SEM and transmission electron microscopy (TEM).

The samples were successfully synthesized as a single-phase apatite, and crystallization of apatite was enhanced during heating. The results obtained in this study show that the kinetics between different direct and inverse process showed different reactivities, in the presence of varying pH. Compared with the two methods, the inverse method have higher kinetic in the formation of hydroxyapatite silicate because of the difference in lattice parameters. The grain size of Si-HA samples is clearly finer than that of pure HA sample and this decreases with increasing Si content. The growth of HA nanorods with temperature can be described by "oriented attachment". According to this theory the adjacent HA crystallites would coalesce in one particular direction on the (1 1 0) high energy planes, creating templates to form elongated rod-like structure. Fourier Transform Infrared Spectroscopy analysis reveals, the silicon incorporation to hydroxyapatite lattice occurs via substitution of silicate groups for phosphate groups. Substitution of phosphate group by silicate in the apatite structure results in a increase in the lattice parameters in both a-axis and c-axis of the unit cell.

Indexing terms/Keywords

Silicon-substituted hydroxyapatite; precipitation aqueous ; Morphology; pH

Academic Discipline And Sub-Disciplines

Biomaterials

SUBJECT CLASSIFICATION

Chemistry

TYPE (METHOD/APPROACH)

Experimental study Silicon-substituted hydroxyapatite

Council for Innovative Research
Peer Review Research Publishing System
Journal: Journal of Advances in Chemistry
Vol. 9, No. 3
editorjaconline@gmail.com
www.cirworld.org/journals

1. INTRODUCTION

Hydroxyapatite (HA, $Ca_{10}(PO_4)_6(OH)_2$) ceramics, the major component of human hard tissues[1], are widely used for bone substitutes in orthopedic and dental clinics in the forms of granules, porous or solid bodies, and finer particles [2], due to its excellent biocompatibility and ability to form a direct chemical bond with hard tissues [3] and [4]. However, HA shows a low bioactive property due to its low resorbability [5] and poor mechanical property[6]. The bioactive behavior of HA has been improved by substituting certain ions in the apatite structure [5], [7] and [8]. It is well understood that minor and trace elements are associated with the properties of biological apatites and they play a major role in the biochemistry of bone, enamel and dentin [9] and [10]. Silicon is one of the trace elements known to be essential in biological processes, while its incorporation in the HA lattice is considered to be a potential method for improving the bioactivity of (HA). As long ago as the 1970, Carlisle [11] and [12] pointed out the importance of Si(IV) in metabolic processes associated with bone formation and calcification, and Gibson et al. [13] reported that silicon-containing hydroxyapatite (Si-HA) enhanced and stimulated osteoblast-like cell activity in vitro. Moreover, Porter and al. [14] mentioned a higher in vivo dissolution rate of SiHAp than that of pure HAp, while Hing and al. [15] reported that Si-HA with 0.8 wt.% Si gave an optimal response in vivo to stimulate both bone-forming and bone-resorbing cells.

Silicon-substituted hydroxyapatite (Si-HA) has been prepared by using various processing techniques in powdered form, sol–gel, hydrothermal, solid state reaction [16], magnetron sputtering [17] and [18], electrospraying [19] and an aqueous precipitation method [20], by different Si sources and different Si contents (0–2 wt.%) [7], [21] and [22]. A research work [22] reported that with Si content substitution higher than 2 wt.%, the original structures of HA was destabilized and secondary phases such as α-TCP.

In recent years, several research works in our group have been devoted to the synthesis of hydroxyapatite in polyol medium [23] and the study of their mechanical behaviour in relation to their biocompatibility. It involves the compaction of the nanoparticles by Spark Plasma Sintering (SPS) process[24].

The aim of this research is to study the effect of pH and the method of inverse and direct synthesis of the maximum incorporation of silicon in the hydroxyapatite without destabilizing the apatite network and the size of grains by precipitation method aqueous.

2. MATERIALS AND METHODS

Of Silicon-substituted hydroxyapatite Si-HA samples were prepared via an aqueous precipitation reaction. The amounts of reactants were calculated on the assumption that silicon would substitute for phosphorus, according to the formula proposed by Gibson and al. [20]: $Ca_{10}(PO_4)_{6-x}(SiO_4)_x(OH)_{2-x}\square_x$ (Si-HA), where x varies from 0 to 2 and □ expresses the anionic vacancies generated.

Indeed, the Si-HA powder was synthesized with two different processes (direct or inverse) and with variation of the pH (9, 8, 7) on the hypothesis that silicon would perfectly substitute into a less basic medium. The procedures are described in detail as follows.

Both pure HA powders were prepared one by inverse mode is to add drop by drop of 0.01796 mol $(NH4)_2HPO_4^{2-}$ (ammonium dihydrogen phosphote, 99.9% pure extra, acros, organics) in a solution of 0.02998 mol Ca $(NO_3)_2$ 4 H_2O (calcuim nitrate tetrahydrate, 99% purity, acros, organics), and for the direct mode, This process consists in pouring a solution containing the cations of Ca^{2+} (calcium nitrate) drop by drop on a solution containing anions PO_3^{4-} (diammonium phosphate $(NH_4)_2HPO_4$). The amount of reagents was calculated in order to obtain a Ca/P molar ratio which is equal to the stoichiometric HA value of 10/6. After the addition of an ammonia solution to adjust the pH of the solution at 10, with a temperature of 100°C, we left the solution for maturation, during 30 min. After cooling, the product was filtered and washed with ethanol in order to remove any other residues before being dried in an oven at 100 °C for 12 h.

Six compositions of Si-HA powder was synthesized with two different factors, the direct or inverse mode, and the variation of pH 9, 8, 7, keeping the same silicon content of added, designated as 9Si-HA, 8Si-HA and 7Si-HA (direct or inverse) respectively. Si-substituted HA (Si-HA) was synthesized, with the same protocol of HA and The amount of reagents were calculated based on a stoichiometric HA, Ca/(P + Si) molar ratio = 10/6, 0.02998 mol of Ca $(NO_3)_2$, $4H_2O$ and a homogeneous solution of 0.011973 mol (NH_4) $2HPO_4$ with of 0.005987 mol Na_2SiO_3 (soduim silicate, 99% purity, acros, organics).

The as-synthesized powders were characterized using an X-ray diffractometer(Philips, CuKa). Besides, the structural information was obtained starting from a powder diagram collected in the angular field 5–110 in 2h with an angular step of 0.04 (2h) and counting time of 5 s. The XRD peak broadening enables us to measure the crystallite size in a direction perpendicular to the crystallographic plane, if the broadening arises entirely as a result of size effects. The crystallite size (d)(hkl) perpendicular to a crystallographic plane (hkl) can be evaluated by measuring the full width at half maximum (FWHM) according to the Scherrer formula:[25]

$$(d)\ (hkl) = K\lambda / B \cos\theta\ (hkl)$$

Where (d) is the crystallite size (nm), K is the shape factor (K is 0.9 when the particles are spherical), λ is the wavelength of the X-rays (k = 1.54056 Å for Cu Ka radiation), B is the FWHM (rad) and θ (hkl) is the Bragg's diffraction angle (°).

With regard to the FT-IR spectra (JASCO 420), they were recorded in the range of 400–4000 cm^{-1} using KBr pellet technique.

The measurement of specific surface were conducted in the process of adsorption into multi-layer of nitrogen gas at low temperature, by means of an automatic sorpiometer (Quantachrome Autosorb AI-C) and according to the theory of BRUNAUER, EMETT, and TELLER (BET).

The size and morphology of the particles as well as the microstructure of the consolidated samples were studied using a JEOL-2011 transmission electron microscope (TEM) operating at 200 kV and Field emission scanning electron microscope (FE-SEM). The samples were coated with a thin layer of gold (Au) by sputtering and then the microstructures were observed using a scanning electron microscope that operate at the acceleration voltage of 15 kV. The elemental composition of the powders was analyzed using energy dispersive X-ray (EDX) (Bruker axes) attached to the field emission scanning electron microscope. The TEM samples of the powders were prepared by dropping an absolute ethanol dispersion of the nanopowders on carbon-coated copper grid. The morphology and physical characteristic of the powder is carried outusing the transmission electron microscope (TEM). Actually, after having passed in ultrasounds bath to separate the particles, the suspension was put on the grid of observation to the TEM.

The chemical formula is determined by dosing chemical elements (table5). The type of dosage of the silicate is gravimetric [26], the reminder the two insolubilization of the silicate by hydrochloric acid and perchloric acid. After cooling, the product was filtered and washed with water in order to remove any other residues before being dried in an oven at 1000°C for 2 h. Calcium was determined by complexometric titration with ethylene diamine tetra-acetic acid [27]. Phosphate was de-termined by colorometry after complexation with phosphovanado-molybdate [28]. The absorbance is measured at 460 nm, and corresponding to the maximum of phosphate ion concentration in the powder

3. RESULTS AND DISCUSSION

3.1 XRD analysis

Fig. 1 shows the XRD patterns of the as-synthesized HA and Si-HA powders, which are described to phase with for a hexagonal crystal system, space group of P63/m (No. 176). The identification of the phases and the lattice constants (c and a) was achieved by crystallographic software. A single HA phase was identified in all specimens by using the International Center for Diffraction Data (ICDD) data bank [29]. The XRD peaks of Si-HA show increasing broadening and decreasing intensity with increasing Si content (Fig. 1(c)–(h)). This is attributed to a loss of crystallinity by the isomorphous substitution of PO_4^{3-} by SiO_4^{4-} during synthesis [28].

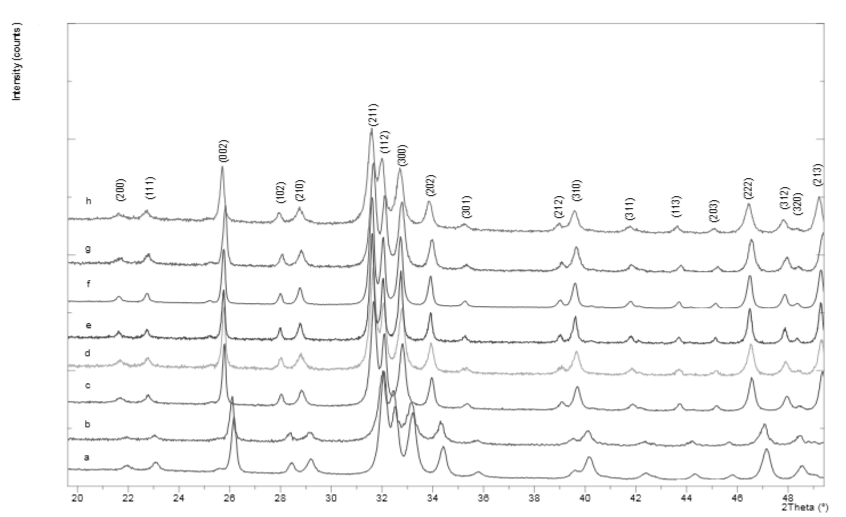

Fig. 1 **XRD patterns of the as-synthesized HA and Si-HA powders: (a) pure HA direct, (b) pure HA inverse, (c) 9Si-HA direct, (d) 9Si-HA inverse, (e) 8Si-HA direct, (f) 8Si-HA inverse, (g) 7Si-HA direct, (h) 7Si-HA inverse**

After heat treatment at 450 °C for 20 h, pure HA and Si-HA a different were formed, no secondary phases are detected (Fig. 2). Comparison of these two figures reveals a considerable improvement of the crystallinity and microstrain in the heat-treated material, as it is shown by the diffraction peaks profile and decrease of the full-width at half-maximum. The lattice parameters of the heat-treated HA, 9Si-HA,8Si-HA and 7Si-HA(direct or inverse) samples are listed in Table 1 and 2,respectively. The lattice constants both a and c increased gradually With decrease of the pH, which means that Si has been successfully incorporated into HA powders. It can be seen that the lattice parameters of Si-HA of All the powders synthesized by the inverse method showed relatively higher than that of by the direct method .

Table 1. Lattice parameters of HA and Si-HA direct samples after heat-treated at temperature of 450°C, Crystallite size (CS), shape factor CS(002)/CS(300) and specific surface area (SSA)

samples	Lattice parameters(A°)		Crystallite size(nm)		Shape factor CS(002)/CS(300)	SSA (m^2g^{-1})
	a	c	(002)	(300)		
pure HA direct	9.4302	6.8803	52.2	27.3	1.91	38.6
9Si-HA direct	9.4520	6.9076	55	25	2.20	43.9
8Si-HA direct	9.4619	6.9185	54	23.7	2.28	45.2
7Si-HA direct	9.4845	6.9326	49.1	21.3	2.31	48.9

Table 2. Lattice parameters of HA and Si-HA inverse samples after heat-treated at temperature of 450°C, Crystallite size (CS), shape factor CS(002)/CS(300) and specific surface area (SSA)

samples	Lattice parameters(A°)		Crystallite size(nm)		Shape factor CS(002)/CS(300)	SSA (m2g-1)
	a	c	(002)	(300)		
pure HA inverse	9.4302	6.8806	58.6	33.9	1.73	40.4
9Si-HA inverse	9.4532	6.9104	48.5	25.2	1.92	44.09
8Si-HA inverse	9.4704	6.9226	45	23.2	1.94	47.9
7Si-HA inverse	9.5021	6.9433	40.3	19.3	2.08	49.7

From results, a compromise can be established between two different processes 7Si-HA direct or 7Si-HA inverse, in Table 3. The results obtained in this study show that the kinetics between different direct and inverse process showed different reactivities, in the presence of varying pH. Compared with the two methods, the inverse method have higher kinetic in the formation of hydroxyapatite silicate because of the difference in lattice parameters (Table 3).

Table 3. Lattice parameters of 7Si-HA direct and 7Si-HA inverse samples after heat-treated at temperature of 450°C, Crystallite size (CS) , shape factor CS(002)/CS(300) and specific surface area (SSA)

samples	Lattice parameters(A°)		Crystallite size(nm)		Shape factor CS(002)/CS(300)	SSA (m2g-1)
	a	c	(002)	(300)		
7Si-HA direct	9.4845	6.9326	49.1	21.3	2.31	48.9
7Si-HA inverse	9.5021	6.9433	40.3	19.3	2.08	49.7

This behavior can be explained by a poor medium OH^- ions which allows the substitution of PO_4^{3-} by SiO_4^{4-} according to the substitution mechanism proposed by Gibson et al. [11] including OH^- vacancies, On the basis of the charge balance, which it has contributed to the increase of the lattice parameters of Si-HA [30], [31] and [32]. As a result, the increase in the lattice parameters of Si-HA resulted in a slight shift of the Si-HA peaks to a lower Bragg's angle compared to pure HA, as shown in Fig. 2.

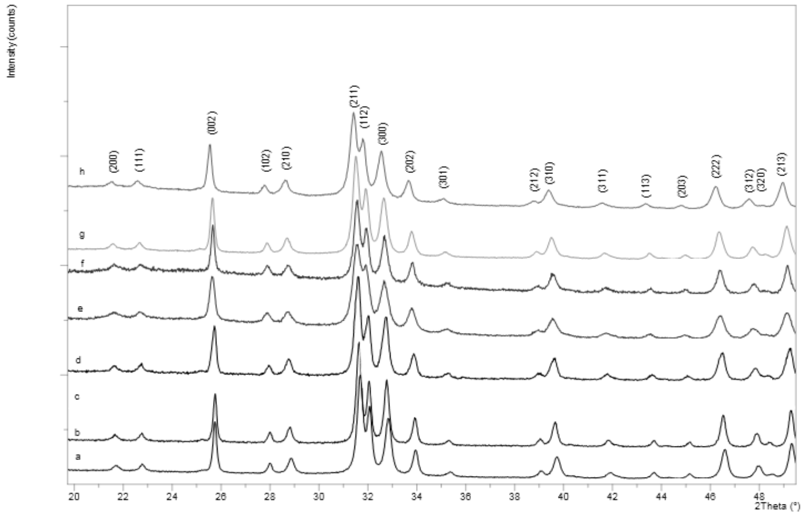

Fig. 2 XRD patterns of HA and Si-HA powders after heat-treatment at 450 °C: (a) pure HA direct, (b) pure inverse, (c) 9Si-HA direct, (d) 9Si-HA inverse, (e) 8Si-HA direct, (f) 8Si-HA inverse, (g) 7Si-HA direct, (h) 7Si-HA inverse

Table1 list the estimated crystallite size (CS) by the scherrer equation, using the (0 0 2) and (300) diffraction and SSA of HA and Si-HA. Those apatite crystallites were almost same in size, shape factor CS (002)/CS (300), and SSA, where a small increment of each property was found, which was compatible with the results by inverse method (Table2).

However, some differences on the XRD patterns can be appreciated with increasing silicon content, namely a progressive broadness of the apatite maxima, the decrease attributable to the (3 0 0) and (2 0 2) reflections can be distinguished from the background, as shown in Fig. 3. This broadening effect can be explained not only by considering the great degree of distortion generated in the structure due to the substitution of view the PO_4^{3-} source by view the SiO_4^{4-} source groups and the creation of vacancies in the OH^- site, but also by a decrease in the crystal size, as previously observed in HA-Si in powder form [20] and [30]. This decrease has been established to affect, particularly, (0 0 1) planes, causing the growth perpendicular to the [0 0 1] direction to be hindered in the presence of silicon, resulting in more needle-shaped crystallites [16].

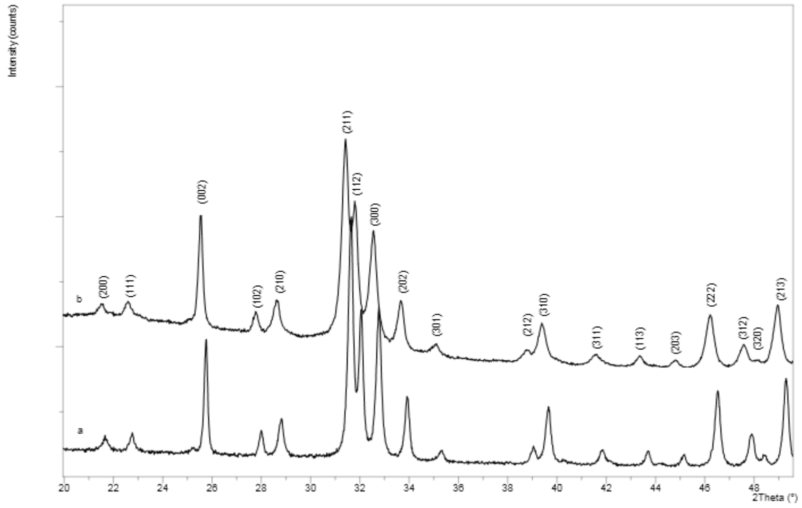

Fig. 3. Peak shift for HA and Si-HA samples with increasing silicon content after heat-treatment at 450 °C: (a) pure HA inverse, (b) 7Si-HA inverse

3.2 FTIR analysis

FTIR spectroscopy was used to study the effect of the silicon substitution on the hydroxyl and phosphate bands of HA. Fig. 4 confirms the formation of samples HA and Si-HA of the as-prepared state.

A weak band of CO_3^{2-} was detected in the region around at 1417–1481 cm^{-1} and a very weak one at 870 cm^{-1}. However, the FTIR spectra indicate that all the samples (with and without Si) contain carbonate groups substitution in the apatite crystal lattice can occur in either the hydroxyl or the phosphate sites, designated as A or B type, respectively [33] in HA powder [34], [35], possibly formed by the dissolution of CO_2 gas during the producing process [36].

In fact, a similar decrease in the intensity of OH^- signals was also observed due to the substitution CO_3^{2-} and SiO_4^{4-} ions for PO_4^{3-} would create an OH^- loss needed to compensate the charge balance, thus resulting in the weak of OH^- signal [37].

The spectra of as-synthesized HA/HA-Si also show the vibrational displacement of the mode present for PO_4^{3-} group at about 963 -961 cm^{-1}, 1101–1092 cm^{-1}, 1033–1030 cm^{-1} can be attributed to the major absorption modes of the phosphate groups, the O–P–O bending mode and for P–O stretching vibration modes of 602–600 cm^{-1} and 566–562 cm^{-1}, respectively [38].The stretching mode of OH^- ions was observed at 3570, 3434 cm^{-1} due to the presence of an organized water structure in HA. The bending mode of OH^- group at 1629 cm^{-1} belonged to the H_2O molecules. The libration mode for OH^- at 632 cm^{-1} was the structural band of HA. All the results were very similar to those reported in the literature [39].

In Another side, the silicon substitution results are observed in three additional peaks about at 1220 -1230 cm^{-1}, 630–640 cm^{-1} and 450–480 cm^{-1} in the Si-HA samples, respectively, are related to SiO_4^{4-} group [40] and [41]. But, the observation of the bands Si–O–Si mode around 634 cm^{-1} is complicated due to the overlapping with the OH^- characteristic bands. In fact, a similar decrease in the intensity of OH^- signals was also observed due to the substitution of SiO_4^{4-} in lattice of HA, point out the appearance of peak. This suggests that phosphate site was substituted by Si in the HA structure [42] and [43]. Further these vibrations modes, which fundamentally correspond to the stretching modes, become wider and less defined in samples containing silicon.

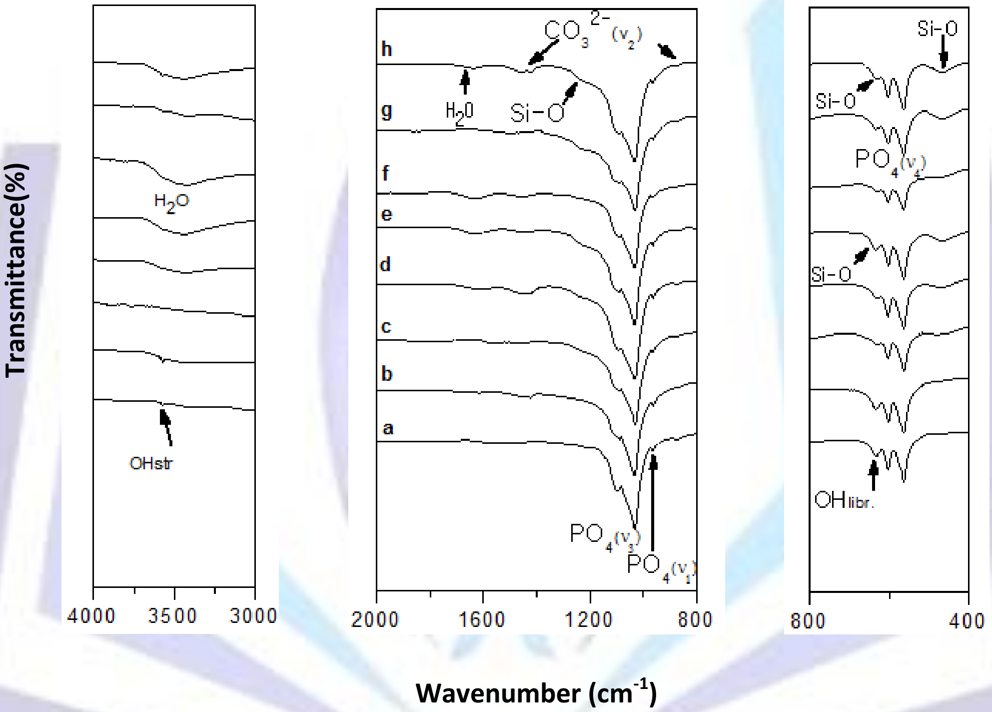

Fig. 4. FT-IR spectra of the as-synthesized HA and Si-HA powders: (a) pure HA direct, (b) pure HA inverse, (c) 9Si-HA direct, (d) 9Si-HA inverse, (e) 8Si-HA direct, (f) 8Si-HA inverse, (g) 7Si-HA direct, (h) 7Si-HA inverse

The FTIR spectra of the heat-treated powders at temperature of 450 °C are quite similar, where Fig. 5 is taken as the representative spectra. Nonetheless, these spectra show significant difference from the as-synthesized samples. The most notable effect of Si substitution on the FTIR spectrum of HA is the decrease in both the PO_4^{3-} group bands, and a similar decrease in the intensity of the OH^- group bands at 631 cm^{-1} and 3572 cm^{-1} compared to the as-synthesized samples is reduced and the carbonate peaks have disappeared. On the other hand The modification of the PO_4^{3-} source bands in the presence of silicon could be associated with the incorporation of silicate ions into some phosphate sites of the lattice, which provoke changes in the bonding and symmetry of the PO_4^{3-} source groups. Examples representative with HA/ 7Si-HA (inverse) are illustrated in table. 4, of the vibrational displacement of the mode present for PO_4^{3-}, OH^- and SiO_4^{4-} group.

Table 4. Mode of the vibrational for PO_4^{3-}, OH^- and SiO_4^{4-} group of HA and Si-HA inverse samples after heat-treated at temperature of 450°C

Samples	PO_4^{3-}				OH^-		SiO_4^{4-}
	υ_1	υ_2	υ_3	υ_4	υ_S	υ_L	
HA inverse	963	-	1101 1033	602 566	3570	632	-
7Si-HA inverse	961	-	1092 1030	600 562	-	-	1220-1230 630-640 450-480

This behavior was associated with the incorporation of Si in the HA lattice, i.e. the incorporation of SiO_4^{4-} into the PO_4^{3-} group and the loss of OH^- group in order to compensate for the extra negative charge of the SiO_4^{4-} group [22] and [44]. Another research work [21] also stated that the negative charge of the SiO_4^{4-} ions substituting PO_4^{3-} is balanced by the creation of hydroxide vacancies, leading to the following chemical formula of Si-HA, according to the formula proposed by results RX and IR:

$Ca_{10}(PO_4)_{6-x}(SiO_4)_x(OH)_{2-x}\square_x$ with $0 \le x \le 2$

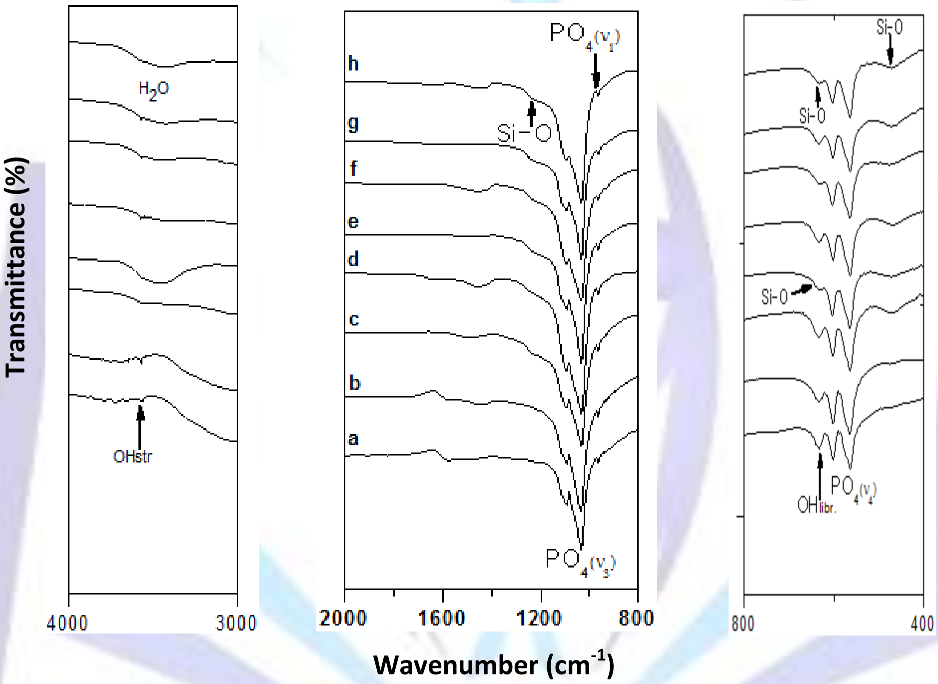

Fig. 5. FT-IR spectra of HA and Si-HA powders after heat-treatment at 450 °C: (a) pure HA direct, (b) pure HA inverse, (c) 9Si-HA direct, (d) 9Si-HA inverse, (e) 8Si-HA direct, (f) 8Si-HA inverse, (g) 7Si-HA direct, (h) 7Si-HA inverse

3.3 The chemicals analysis

The elemental quantity analysis the all samples given the concentrations of Ca^{2+}, PO_4^{3-} and SiO_4^{4-} and the chemical formulas in the table 5,The Ca/P ratio increased with the Si content, while the Ca/(P + Si) ratio remained almost constant 1.67. It also confirmed that SiO_4^{4-} were successfully loaded into the HA powders, and the silcon content increased as the content of PO_4^{3-} decreased. The chemical compositions of wet-chemically derived HA and Si-HA was differed from the nominal composition. The increase in lattice constants as shown in table.1, 2, the amount of Si in of samples is much lower than the starting value, the silicate species which could not totally be incorporated in the apatite structure remain in mother liquors after precipitation [8]. The remaining Si suggests that the competition arising between the SiO_4^{4-} and OH^- ions occupies the sites.We can also see that the concentration of the calcium in the pure HA and the Samples containing silicon noted constant. These results are in good accord with the previous results by RX and FTIR. Which is confirmed to the chemical formula of Si-HA proposed by Gibson and al.[20]:

$Ca_{10}(PO_4)_{6-x}(SiO_4)_x(OH)_{2-x}\square_x$ (Si-HA)

Where x varies from 0 to 2 and □ expresses the anionic vacancies generated.

Table 5. The elemental quantity analysis the all samples after heat-treated at temperature of 450°C and the chemical formulas

Samples	The concentrations			The chemical formulas
	$\%Ca^{2+}$ ± 1	$\%PO_4^{3-}$ ± 1	$\%SiO_4^{4-}$ ± 0.4	$Ca_{10}(PO_4)_{6-x}(SiO_4)_x(OH)_{2-x}\square_x$
HA direct	39.544	56.808	0	$Ca_{10}(PO_4)_6(OH)_2$
HA inverse	39.544	56.808	0	$Ca_{10}(PO_4)_6(OH)_2$
9Si-HA direct	40.115	48.841	9.024	$Ca_{10}(PO_4)_{5.050}(SiO_4)_{0.950}(OH)_{1.050}\square_{0.950}$
9Si-HA inverse	40.686	48.266	9.575	$Ca_{10}(PO_4)_{4.998}(SiO_4)_{1.012}(OH)_{0.998}\square_{1.012}$
8Si-HA direct	40.876	45.202	12.615	$Ca_{10}(PO_4)_{4.654}(SiO_4)_{1.346}(OH)_{0.654}\square_{1.346}$
8Si-HA inverse	41.066	43.861	14.241	$Ca_{10}(PO_4)_{4.494}(SiO_4)_{1.506}(OH)_{0.494}\square_{1.506}$
7Si-HA direct	41.256	39.992	18.413	$Ca_{10}(PO_4)_{4.065}(SiO_4)_{1.935}(OH)_{0.065}\square_{1.935}$
7Si-HA inverse	41.447	39.418	19.127	$Ca_{10}(PO_4)_4(SiO_4)_2\square_2$

3.4 Morphologies of Si–HA nanoparticles powders

The EDX patterns of the nano HA and Si–HA composite powders are shown in Fig. 6. The elemental composition of the powders was mainly Ca, P, O and O, P, Ca and Si, respectively. A small amount of C was also observed due to the dissolution of CO_2 gas during the producing process. The Si signals in the elemental mapping gradually became stronger with the increase of silicon incorporation content and decrease of the pH, which means that Si has been successfully, incorporated into HA powders. All the powders synthesized by the direct method showed a lower silicon signal in the EDX pattern compared by the inverse method, indicating more Si in the latter. The EDX mapping revealed that the silicon have a different distribution in the entire HA powder, which was compatible with the results RX.

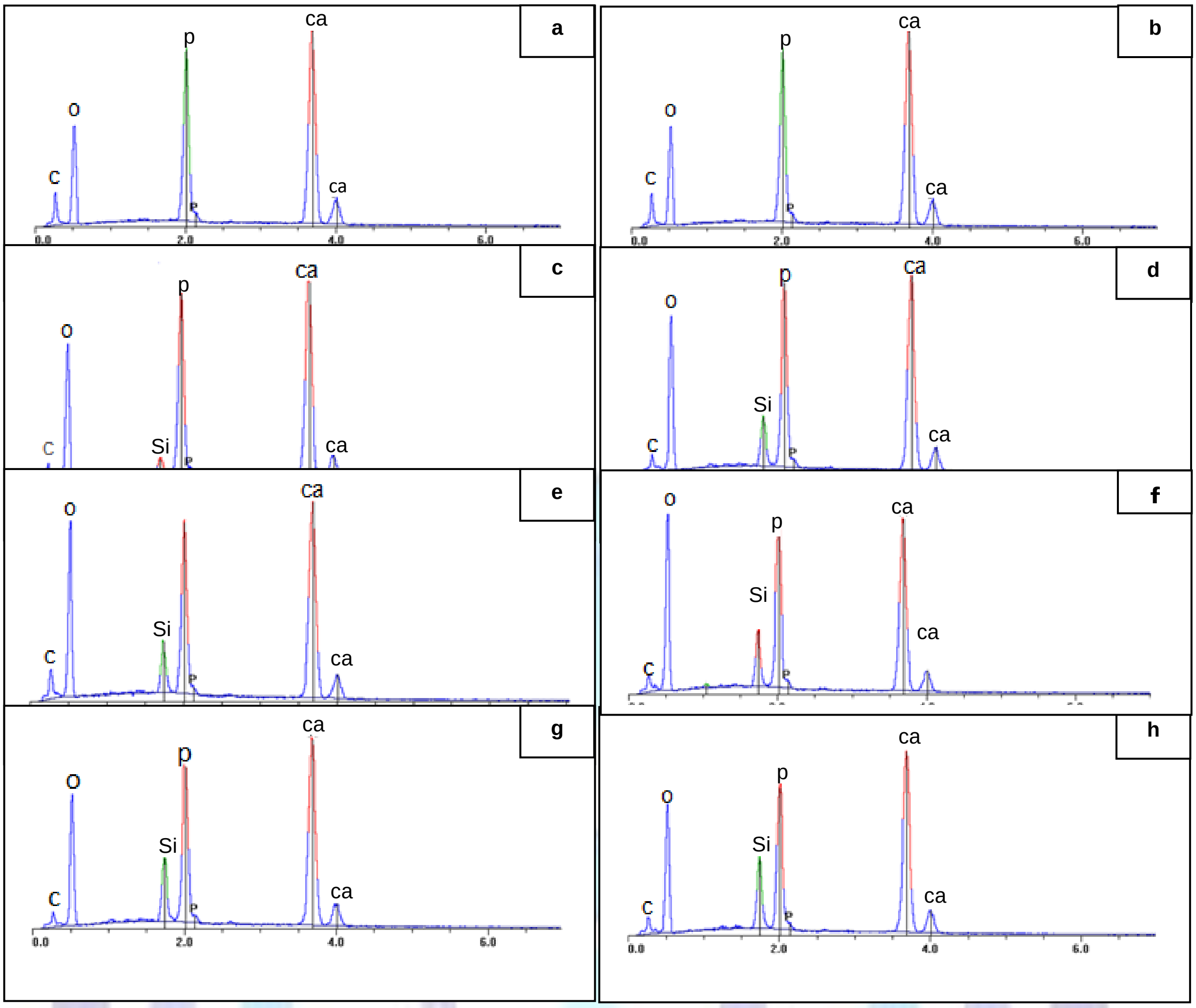

Fig. 6. The EDX patterns of HA and Si-HA powders after heat-treatment at 450 °C: (a) pure HA direct, (b) pure HA inverse, (c) 9Si-HA direct, (d) 9Si-HA inverse, (e) 8Si-HA direct, (f) 8Si-HA inverse, (g) 7Si-HA direct, (h) 7Si-HA inverse

The effect of Si substitution on the grain size samples was studied using SEM of after the heat-treated at 450°C, examples of representative with HA/ 7Si-HA (direct and inverse) are illustrated in Fig. 7. It can be concluded from the images Nanocrystalline Si-HA particles thus obtained present interesting morphological characters varying from platelet to very thin needles. The average length of the 7Si-HA (direct and inverse) rod seems to vary between 300 and 500 nm, while the average diameter was found to be between 50 and 70 nm (see Fig. 7).

The particle size and the morphologies 7Si-HA have no obvious difference for the two types of method direct and inverse, but the latter showed a stronger silicon signal in the EDX pattern (Fig. 6), indicating more Si in the latter. All the powders, including as-received HA and silicon containing HA powders, were in the nanoscale and aggregated together loosely.

Although the present work does not synthesize rods with exact dimensions of HA crystals of teeth, the synthesized nanorods can be used as a substitute in applications where the Si-HA crystals are applied to the surface of proteins and are incorporated into the tooth or bone materials in a biomineralization healing process [45]. Even HA present in human tooth and bone exhibits the form of nano-polycrystalline hexagonal nanorods[46].

There had been many reports on the effect of Si on the grain size of Si-HA. These research works Pollard et al. [47] and Li et al. [48] agreed that the grain size of Si-HA decreases with increasing Si content, and Gibson et al. [49] suggested that a higher value of activation energy (183–205 kJ/mol) was required for the grain growth of Si-HA compared to stoichiometric HA (141 kJ/mol). This indicates that Si effectively impedes the grains from coarsening during the synthesis. This means that of silicon source is another key factor in controlling crystallinity and crystallite size because the thermochemical reaction kinetics of the silicon source may be different.

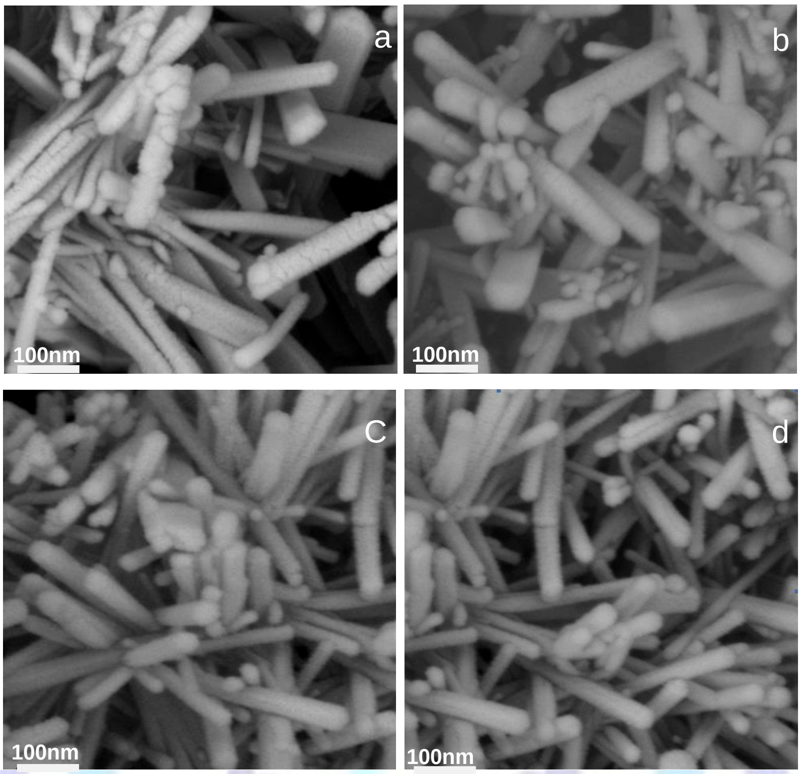

Fig. 7. The SEM image of HA and Si-HA powders after heat-treatment at 450 °C: (a) pure HA direct, (b) pure HA inverse, (c) 7Si-HA direct, (d) 7Si-HA inverse

The resolution TEM (Fig. 8(a), 8(c)) and selected area electron diffraction (SAED) (Fig. 8(b), 8(d)) analyses were performed to determine growth direction of HA-Si nanorods, before and after the heat-treated at 450°C, for the maximum sample of silicon substituted hydroxyapatite in the network (7Si-HA inverse).

Fig. 8(a) and (b) compares the TEM images of Si-HA before and after the heat-treated. The produced nanoparticles are of spherical shape, with a diameter range of 20–30 nm (fig 8(a)). some agglomeration of particles was observed in the powder (Fig. 8(a)). The TEM images in Fig. 8c show nanostructures of 7Si-HA particles that consisted the how those nanosized crystallites aggregated and formed rod-like shaped grains. This agglomeration between particles is attributed to the large surface area and energy associated with nanoparticles.

The inset in Fig. 8b represents selected-area electron diffraction (SAED) pattern of the region of this image: diffuse rings and spots indicate poor crystallinity of 7Si-HA, before the heat-treated. The corresponding pattern is characteristic of a polycrystalline material with diffraction rings that can be indexed to the interplanar distances of an apatite-like structure. The pattern shows the sharp (002) diffraction peak reflection, the elongated nature of the crystals, and the broad diffraction band containing the (211), (112), and (300) diffraction peaks, which is a characteristic of biological apatite. The continuity of the rings in the first selected area diffraction indicates the presence of randomly oriented grains of very fine dimension (Fig. 8d), that indicate more crystallization at the long time heat-treated. These results confirm the obtained TEM results. The domain size presented here agrees with that determined by the XRD analysis and this result confirms that the crystallite size corresponds to a coherent domain size.

The possible nanorod nucleation and growth could be attributed to the relative specific surface energies associated with the different planes of HA crystal or nucleus. These different planes which have different surface energies will determine the amount of OH^- absorbance from the solution [50] and [51]. Furthermore, the growth of Si-HA nanorods with temperature can be described by “oriented attachment” mechanism reported for other ceramics like TiO_2 [52]. According to this theory the adjacent HA crystallites would coalesce in one particular direction on the (1 1 0) high energy planes, creating templates to form elongated rod-like structure.

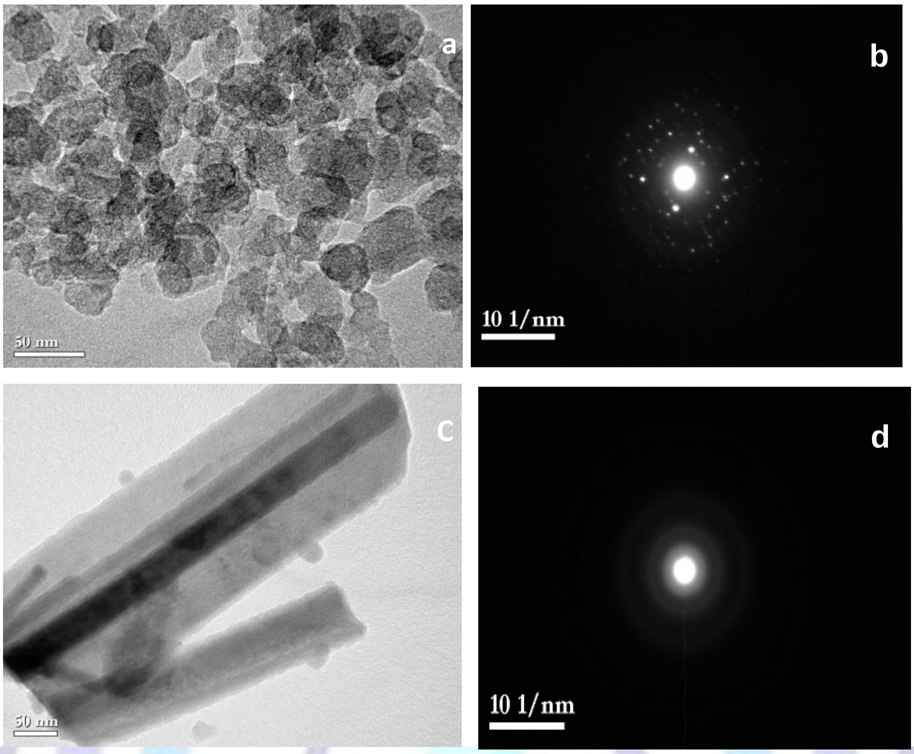

Fig.8. (a) TEM image, (b) SAED patterns of the as-synthesized 7Si-HA powders inverse and (c) TEM image, (d) SAED patterns of the powders7Si-HA inverse after heat-treatment at 450 °C

4. CONCLUSION

In this work, the effects of pH and the process of direct or inverse synthesis was determined by the theoretical maximum of incorporation of Si into the hexagonal apatite structure according to the following formula $Ca_{10}(PO_4)_{6-x}(SiO_4)_x(OH)_{2-x}\square_x$ ($0 \le x \le 2$), by precipitation method aqueous. Rietveld analysis showed the calcined HA-Si powders of high purity, the lattice constants both a and c increased gradually With decrease of the pH, with a unit cell structure adequate ,which was compatible with the results EDX. The results showed that the process inverse could be most effective in the kinetics of silicon-substitute hydroxyapatite formation that the direct method.

Calcination yielded HA-Si nanorod of decreased particle size and crystallinity with decrease of the pH. FTIR showed presence of where silicates are introduced in the phosphate sites with the a similar decrease in the intensity of the OH^- until disappeared. The particle size and morphology was studied using transmission electron microscopy, where the crystallites stick together on high energy plane and template the growth in one particular direction.

REFERENCES

[1] De Groot K. 1983. Bioceramics of Calcium Phosphate CRC Press, Boca Raton, FL.

[2] Legeros, R.Z. and Legeros, J.P. 2008. Hydroxyapatite. In: Kokubo T, editor. Bioceramics and their clinical applications. Cambridge: Woodhead Publishing. 367–94.

[3] Suchanek, W.L., Shuk, P., Byrappa, K., Riman, R.E., TenHuisen, K.S. and Janas, V.F. 2002. Mechanochemical-hydrothermal synthesis of carbonated apatite powders at room temperature. Biomaterials. 23, 699–710.

[4] Wong, J.Y. and Bronzino (Eds.), J.D. 2007. Biomaterials. CRC Press, Boca Raton, Florida.

[5] Maria, V.R. and Daniel, A. 2005. Silicon substituted hydroxyapatite. A method to upgrade calcium phosphate based implants. J. Mater. Chem. 15 , 1509–1516.

[6] Salih, V., Georgiou, G., Knowles, J.C. and Olsen, I. 2001. Biomaterials. 22, 2817.

[7] Balas, F., Pariente, J.P. and Regi, M.V. 2003. In vitro bioactivity of silicon-substituted hydroxyapatites J. Biomed. Mater. Res. 66A , 364–375

[8] Aminian, A., Hashjin, M., Samadikuchaksaraei, A., Bakhshi, F., Gorjipour, F., Farzadi, A., Moztarzadeh, F. and Schmcker, M. 2011. Synthesis of silicon-substituted hydroxyapatite by a hydrothermal method with two different phosphorous sources. Ceram. Int. 37, 1219–2122

[9] Zapanta LeGeros R. 1991. Calcium phosphates in oral biology, medicine. New York: Krager. 82–107.

[10] Smith, D.K. 1994. Calcium phosphate apatites in nature. In: Brown PW, Constantz B, editors. Hydroxyapatite and related materials. Boca Raton, FL: CRC Press. 29–44.

[11] Carlisle, E.M. 1970. Silicon: a possible factor in bone calcification. Science. 167,179–80.

[12] Carlisle, E.M. 1981. Silicon: a requirement in bone formation independent of vitamin D1. Calcif Tissue Int. 33, 27–34.

[13] Gibson, I.R., Huang, J., Best, S.M. and Bonfield, W. 1991. Enhanced in vitro cell activity and surface apatite layer formation on novel silicon-substituted hydroxyapatites.Bioceramics. 12, 191–4.

[14] Porter, A.E., Patel, N., Skepper, J.N., Best, S.M. and Bonfield, W. 2003. Comparison of in vivo dissolution processes in hydroxyapatite and silicon-substituted hydroxyapatite bioceramics. Biomaterials. 24, 4609–20.

[15] Hing, K.A., Revell, P.A., Smith, N. and Buckland, T. 2006. Effect of silicon level on rate, quality and progression of bone healing within silicate-substituted porous hydroxyapatite scaffolds. Biomaterials. 27, 5014–26.

[16] Vallet-Regí, M. and Arcos, D. 2005. Silicon substituted hydroxyapatites. A method to upgrade calcium phosphate based implants. J. Mater. Chem. 15, 1509–1516

[17] Thian, E.S., Huang, J., S.M. Best, Z.H. and Barber, W. 2005. Bonfield,Magnetron co-sputtered silicon-containing hydroxyapatite thin films—an in vitro study. Biomaterials. 26, 2947–2956

[18] Porter, A.E., Rea, S.M., Galtrey, M., Best, S.M. and Barber, Z.H. 2004. Production of thin film silicon-doped hydroxyapatite via sputter deposition. J. Mater. Sci. 39, 1895–1898

[19] Huang, J., Best, S.M., Jayashinghe, S.N., Edirisinghe M.J., Brooks, R.A. and Bonfield, W. 2005. Novel deposition of nano-sized silicon substituted hydroxyapatite by electrospraying. In: Proceedings of the 19th European Conference on Biomaterials, ESB, Sorrento, Italy.

[20] Gibson, I.R., Best, S.M. and Bonfield, W. 1999. Chemical characterization of silicon-substituted hydroxyapatite. J. Biomed. Mater. Res. 44, 422–8.

[21] Palard, M., Champion, E. and Foucaud, S. 2008. Synthesis of silicate hydroxyapatite $Ca10(PO4)6-x(SiO4)x(OH)2-x$. J. Solid State Chem. 181, 1950–1960

[22] Kim, S.R., Lee, J.H., Kim, Y.T., Riu, D.H., Jung, S.J., Lee, Y.J., Chung, S.C. and Kim, Y.H. 2012. Synthesis of Si, Mg substituted hydroxyapatites and their sintering behaviors. Biomaterials. 23, 1389–1398

[23] Mechay, A., Elfeki, H., Schoenstein, F. and Jouini, N. 2012. Nanocrystalline hydroxyapatite ceramics prepared by hydrolysis in polyol medium. Chemi. Phys. Lett. 541, 75-80

[24] Mechay, A., Elfeki, H., Schoenstein, F. and Jouini, N. 2014. Nanocrystalline Hydroxyapatite Ceramics Prepared by Hydrolysis in Polyol Medium, Microstructure and Mechanical Properties after Spark Plasma Sintering. Journal of Advances in Chemistry. 1085-1092.

[25] Azaroff, L.A. 1986. Elements of X-ray crystallography, McGraw-Hill, New York. 38–42

[26] Amer . Soc. Test. Mater. , (A.S.T.M.) , Chemical analysis of refractory materials 3, 492 , (1949) .

[27] Charlot, G. 1966. Les Méthodes de la Chimie Analytique, 5éme édition, Masson, Paris.

[28] Gee, A. and Deitz, V.R. 1953. Anal. Chem. 25 , 1320.

[29] Kay, M.I., Young, R.A. and Posner, A.S.1964. Nature. 204, 1050.

[30] Tang, X.L., Xiao, X.F. and Liu, R.F. 2005. Structural characterization of silicon-substituted hydroxyapatite synthesized by a hydrothermal method. Mater. Lett. 9, 3841–3846

[31] Sprio, S., Tampieri, A., Landi, E., Sandri, M., Martorana, S., Celotti, G. and Logroscino, G. 2006. Physico-chemical properties and solubility behavior of multi-substituted hydroxyapatite powders containing silicon. Mater. Sci. Eng. C. 28, 179–187

[32] Xu, J.L. and Khor, K.A. 2007. Chemical analysis of silica doped hydroxyapatite biomaterials consolidated by a spark plasma sintering method. J. Inorg. Biochem. 101, 187–195

[33] El Feki, H., Rey, C. and Vignoles, M. 1991. Calcif. Tissue Int. 49, 269.

[34] El Feki, H., Khattech, I., Jemal, M. and Rey, C. 1994. Thermochim. Acta. 237, 99.

[35] El Feki, H., Savariault, J.M. and Ben Salah, A. 1999. J. Alloys Compd. 287, 114.

[36] Sun, Y.G., Gates, B., Mayers, B. and Xia, Y.N. 2002. Crystalline silver nanowires by soft solution processing. Nano Letters 2. 165–168.

[37] Kannan, S., Vieira, S. I., Olhero and al., S. M. 2011. Synthesis, mechanical and biological characterization of ionic doped carbonated hydroxyapatite/β-tricalcium phosphate mixtures. Acta Biomaterialia. 7, 1835–1843.

[38] Fowler,B.O. 1974. Infrared studies of apatites, vibrational assignments for calcium, strontium and barium hydroxyapatites utilizing isotopic substitution. Inorg. Chem. 13, 194–207

[39] Rehman, I. and Bonfield,W. 1997. Characterization of hydroxyapatite and carbonated apatite by photo acoustic FTIR spectroscopy. Journal of Materials Science: Materials in Medicine. 8, 1–4

[40] KALT, A. and WEY, R. 1968. Compounds interlayer of hydrated crystalline silica. Bull. Gr. Fr. Argiles. 20, 205-214.

[41]TARTE, P. 1962. Study of silicates by infrared spectrometry. Bull. Soc. Fr. Céram., D. 553 : 13-34.

[42] Best, S.M., Bonfield, W., Gibson, I. and Welwyn, R. 2001. Silicon-substituted apatites and process for the preparation there of. United States Patent.

[43] Tian, T., Jiang, D., Zhang, J. and Lin,Q. 2008. Synthesis of Si-substituted hydroxyapatite by wet mechanochemical method. Mater. Sci. Eng. C. 28 57–63.

[44] Bianco, A., Cacciotti, I., Lombardi, M. and Montanaro, L. 2009. Si-substituted hydroxyapatite nanopowders: synthesis, thermal stability and sinterability. Mater. Res. Bull. 44, 345–354

[45] Ralf, N., Hans-Josef, S. and & Volker, K. 2006. Rod shaped apatite crystals having a specific length-to-width ratio. US Patent. 482.

[46] Cuisinier, F. and Robinson,C. 2007. The structure of teeth: Human enamel crystal structure ,M. Epple, E. Baeuerlein (Eds.). Handbook of biomineralization: Medical and clinical aspects, Wiley-VCH, Weinheim. 177–182.

[47] Palard, M., Combes, J., Champion, E., Foucaud, S., Rattner, A. and Bernache-Assollant, D. 2009. Effect of silicon content on the sintering and biological behavior of $Ca10(PO4)6-x(SiO4)x(OH)2-x$ ceramics. Acta Biomater. 5, 1223–1232.

[48] Li, X.W., Yasuda, H.Y. and Umakoshi, Y. 2006. Bioactive ceramic composites sintered from hydroxyapatite and silica at 1200 °C: preparation, microstructures and in vitro bone-like layer growth. J. Mater. Sci. Mater. Med. 17, 573–581.

[49] Gibson, I.R., Best, S.M. and Bonfield, W. 2002. Effect of silicon substitution on the sintering and microstructure of hydroxyapatite. J. Am. Ceram. Soc. 85, 2772–2777

[50] Li, W.J., Shi, E.W., Zhong, W.Z. and Yin, Z.W. Growth mechanism and growth habit of oxide crystals. Journal of Crystal Growth. 203, 186–196

[51] Liu, J., Li, K., Wang, H., Zhu, M. and Yan, H. 2004. Rapid formation of hydroxyapatite nanostructures by microwave irradiation. Chemical Physics Letters. 396, 429–432.

[52] Nian, J.N. and Teng, H. 2006. Hydrothermal synthesis of single-crystalline anatase TiO2 nanorods with nanotubes as the precursor. The Journal of Physical Chemistry B. 110, 4193–4198.